Cytotherapy 000 (2024) 1–10

Contents lists available at ScienceDirect

CYTOTHERAPY

journal homepage: www.isct-cytotherapy.org

Full-length article

Extracellular vesicles from adipose mesenchymal stem cells target inflamed lymph nodes in experimental autoimmune encephalomyelitis

Ermanna Turano[1], Ilaria Scambi[1], Roberta Bonafede[1], Silvia Dusi[2], Gabriele Angelini[2], Nicola Lopez[2], Giulia Marostica[3], Barbara Rossi[2], Roberto Furlan[3], Gabriela Constantin[2], Raffaella Mariotti[1], Bruno Bonetti, MD, PhD[4,*]

[1] *Department of Neuroscience, Biomedicine and Movement Sciences, University of Verona, Verona, Italy*
[2] *Division of General Pathology, Department of Medicine, University of Verona, Verona, Italy*
[3] *Clinical Neuroimmunology Unit, Institute of Experimental Neurology, San Raffaele Scientific Institute, Milan, Italy*
[4] *Neurology Unit, Azienda Ospedaliera Universitaria Integrata Verona, Verona, Italy*

ARTICLE INFO

Article History:
Received 7 May 2023
Accepted 26 December 2023
Available online xxx

Key Words:
adipose mesenchymal stem cells
EAE
extracellular vesicles
multiple sclerosis
stem cells
superparamagnetic iron oxide nanoparticles

ABSTRACT

Background aims: Adipose mesenchymal stem cells (ASCs) represent a promising therapeutic approach in inflammatory neurological disorders, including multiple sclerosis (MS). Recent lines of evidence indicate that most biological activities of ASCs are mediated by the delivery of soluble factors enclosed in extracellular vesicles (EVs). Indeed, we have previously demonstrated that small EVs derived from ASCs (ASC-EVs) ameliorate experimental autoimmune encephalomyelitis (EAE), a murine model of MS. The precise mechanisms and molecular/cellular target of EVs during EAE are still unknown.
Methods: To investigate the homing of ASC-EVs, we intravenously injected small EVs loaded with ultra-small superparamagnetic iron oxide nanoparticles (USPIO) at disease onset in EAE-induced C57Bl/6J mice. Histochemical analysis and transmission electron microscopy were carried out 48 h after EV treatment. Moreover, to assess the cellular target of EVs, flow cytometry on cells extracted *ex vivo* from EAE mouse lymph nodes was performed.
Results: Histochemical and ultrastructural analysis showed the presence of labeled EVs in lymph nodes but not in lungs and spinal cord of EAE injected mice. Moreover, we identified the cellular target of EVs in EAE lymph nodes by flow cytometry: ASC-EVs were preferentially located in macrophages, with a consistent amount also noted in dendritic cells and CD4+ T lymphocytes.
Conclusions: This represents the first direct evidence of the privileged localization of ASC-EVs in draining lymph nodes of EAE after systemic injection. These data provide prominent information on the distribution, uptake and retention of ASC-EVs, which may help in the development of EV-based therapy in MS.

Introduction

Experimental autoimmune encephalomyelitis (EAE) represents the most used animal model in multiple sclerosis (MS), not only for investigating the pathogenic features but also for identifying new potential therapeutic strategies. MS is a chronic inflammatory degenerative disease with evidence of autoimmune activity toward the central nervous system (CNS), characterized by demyelination and axonal damage [1,2].

Several studies on the use of mesenchymal stem cells (MSCs) in the treatment of EAE have achieved encouraging results, suggesting both peripheral and central mechanisms [3–8]. Experimental evidence has indeed demonstrated that the therapeutic effects of MSCs do not require their engraftment in the CNS but depend on their ability to reach peripheral lymphoid organs as well as to infiltrate sites of injury and inflammation favoring immune regulation and tissue repair, respectively, by the release of extracellular vesicles (EVs) containing modulating factors [6,9–11]. It is clearly confirmed that EVs derived from MSCs (MSC-EVs) maintain some characteristics of their parent-derived cells [12], including an immunomodulatory and neuroprotective role, as demonstrated using *in vitro* and *in vivo* experimental approaches [13–18] and also in EAE [19,20]. In this regard, our group showed that the preventive administration of small EVs derived from adipose mesenchymal stem cells (ASC-EVs) ameliorates chronic EAE by interfering with the integrin-dependent adhesion of activated T

* Correspondence: Bruno Bonetti, Neurology Unit, Azienda Ospedaliera Universitaria Integrata Verona, Verona, Italy.
E-mail address: bruno.bonetti@aovr.veneto.it (B. Bonetti).

https://doi.org/10.1016/j.jcyt.2023.12.007

cells to spinal cord pial vessels and inhibiting the activation of CD4 + T cells in lymph nodes of EAE-induced animals, with consequent reduced production of pro- and anti-inflammatory cytokines [19]. Although the trafficking of stem cells from the systemic circulation has long been characterized, this is not yet known for their derived vesicles.

Contrary to their parent cells, the traceability of MSC-EVs *in vivo* proved to be technically challenging because of their nanosize. Nevertheless, recent advanced techniques are being employed to identify accumulation sites and cell targets of EVs [21–24], resulting in significant improvement in the evaluation of their *in vivo* cell tissue distribution.

In this study, we describe for the first time the delivery of small ASC-EVs labeled with ultra-small superparamagnetic iron oxide nanoparticles (USPIOs) after intravenous injection in EAE-induced mice using histochemical and ultrastructural studies. Starting from the experimental evidence obtained in our previous study, we focused our attention on lymph nodes, identified as the target site of ASC-EV action [19]. The identification of MSC-EV target sites in the early onset of disease represents one of the relevant issues to be addressed to fill the gap between experimental pre-clinical studies and therapy, which currently does not report significant successes [25]. Here we aim to confirm with direct evidence the site of action of ASC-EVs in EAE mice and to identify their cellular targets, which are currently unknown. The ability of ASC-EVs to accumulate preferentially in the secondary lymphoid organs rather than in the sites of injury and inflammation could allow the development of minimally invasive systemic delivery strategies, avoiding the risks related to uncontrolled proliferation and tumor development [26,27]. These results pave the way for the successfully targeted application of ASC-EVs for the treatment of MS and other neurological diseases.

Methods

Cell cultures

Murine ASCs were obtained from inguinal adipose tissue of 6- to 8-week-old C57Bl/6J mice (Charles River Laboratories, Wilmington, MA, USA). The isolation of stromal vascular fraction from the lipoaspirate was carried out as previously described [3]. Briefly, extracellular matrix was digested with collagenase A type I (Roche, Basel, Switzerland) and centrifuged at 1200 × g. The pellet obtained was resuspended and the stromal fraction was collected via sequential centrifugation and filtration steps.

Human ASCs were obtained from lipoaspirates of healthy donors after informed consent, and their extraction was performed as described by Peroni *et al.* [28]. Murine and human ASCs were cultured in complete Dulbecco's Modified Eagle's Medium with 10% fetal bovine serum, 100 U/mL penicillin and 100 μg/mL streptomycin (Thermo Fisher Scientific, Waltham, MA, USA) and incubated at 37°C in 5% carbon dioxide. To reduce inter-donor variability ASCs were obtained from different donors, cultivated separately and pooled together for the experiments. The characterization of adipose-derived MSCs agreed with the MSC standards established by the International Society for Cell & Gene Therapy [29] as previously reported by us [15,30].

The immunophenotypic analysis of murine ASCs was performed using monoclonal antibodies (mAbs) specific for CD106, CD9, CD44, CD80, CD138 and stem cell antigen 1. In addition, the absence of hematopoietic (CD45, CD11c and CD34) and endothelial (CD31) markers was assessed as previously described [10]. All mAbs were purchased from Becton Dickinson (Franklin Lakes, NJ, USA). Isotype-matched antibodies were used as controls. Briefly, ASCs were detached using trypsin/ethylenediaminetetraacetic acid for 5 min, immediately washed with phosphate-buffered saline (PBS) to remove trypsin and resuspended at 10^6 cells/mL. Cell suspension was incubated at 4°C for 10 min with 15% adult bovine serum followed by incubation with the specific mAb at 4°C for 30 min. At least 10 000 events were analyzed by flow cytometry (BD FACSCalibur; Becton Dickinson) using BD CellQuest software (Becton Dickinson). For the immunophenotypic analysis, human ASCs were evaluated for the expression of CD105, CD73, CD29 and CD44 and the lack of hematopoietic and endothelial cell markers as previously described [28,31].

ASC-EV isolation, labeling and characterization

ASC-EVs were isolated from the culture medium of murine ASCs at passage 14–18 as previously described [15,19]. The same protocol was used to extract human ASC-EVs (hEVs) at passage eight to 10 as previously described [32]. ASC-EVs were extracted from a pool of ASC cells derived from different donors to reduce inter-donor variability. Murine ASCs were grown to confluence and incubated with 200 μg iron/mL of USPIOs for 24 h [14,33]. Following USPIO labeling, ASCs were maintained for 48 h in Dulbecco's Modified Eagle's Medium supplemented with 0.5% ultracentrifuged fetal bovine serum to reduce serum contamination. ASC supernatants were collected and small EVs were enriched using a PureExo Exosome Isolation kit (101Bio, Mountain View, CA, USA) following the manufacturer's protocol. The FBS was purified with ultracentrifugation at 120,000 g (Optima Max-E Ultracentrifuge, Beckman Coulter) for 18 hours [34]. The supernatant was collected carefully, to not disturb the visible pellet. The collected supernatant was subjected to 0.2 μm filtration twice and a single 0.1 μm filtration before adding it in the culture medium [35]. The protein content of EVs, USPIO-EVs and hEVs was determined via bicinchoninic acid protein assay of five different extractions. The bicinchoninic acid protein assay (Pierce BCA Protein Assay Kit; Thermo Fisher Scientific) was performed following the manufacturer's protocol. Briefly, EV proteins were incubated with the working reagents at 60°C for 30 min according to the enhanced protocol of the Pierce BCA Protein Assay Kit. Subsequently, protein samples were loaded into each well of a 96-well plate, and the absorbance was measured at 562 nm by a microplate reader (ChroMate; RayBiotech, Peachtree Corners, GA, USA). A standard curve was used to calculate the protein concentration of EV samples. The efficiency of EV labeling and the quantification of USPIO-EV iron nanoparticles were previously reported by our group using several experimental approaches [21].

To confirm EV isolation and purity, 20–30 μg of EVs was eluted with loading buffer, boiled for 5 min and separated in 10% and 12% polyacrylamide gels at 100–150 V. Proteins were transferred onto polyvinylidene difluoride membranes (Immobilon-P; MilliporeSigma, Burlington, MA, USA) for 2 h at 60 V in transfer buffer. Membranes were then blocked with 10% non-fat dry milk for 1 h and incubated with anti-CD9 mAb (1:500; MilliporeSigma), polyclonal anti-HSP70 (1:1000; Santa Cruz Biotechnology, Dallas, TX, USA), anti-TSG101 mAb (1:1000; Abcam, Cambridge, UK) and polyclonal anti-GM130 antibody (1:500; Thermo Fisher Scientific). For hEVs, the presence of human leukocyte antigen (HLA) was evaluated by anti-human HLA mAb (1:500; Thermo Fisher Scientific). After incubation with the appropriate secondary IgG horseradish peroxidase-conjugated antibodies, the membranes were developed with Immobilon Western substrate (MilliporeSigma) and proteins were visualized on autoradiography film (Amersham Hyperfilm; Cytiva, Marlborough, MA, USA).

Size distribution and concentration of isolated EVs were measured by nanoparticle tracking analysis (NTA) using a NanoSight NS300 (Malvern Panalytical, Malvern, UK) equipped with a 488-nm laser and a syringe pump system with a pump speed of 20 μL/s. For the measurements, five video recordings with a duration of 1 min were carried out for each sample diluted 1:100 in PBS. Camera level and detection threshold were set in acquisition and analysis, respectively, in order to achieve a concentration between 20 and 120 particles per frame. NTA 3.4 software (Malvern Panalytical) was used to acquire

and analyze the sample videos. The results are reported as mean ± standard error of the mean of five measurements. For size determination, the data are reported as statistical mode ± standard error of the mean of five measurements. The NTA measurements represents 5 biological replicates of ASC-EVs batches derived from the mean of 3 technical replicates.

EAE induction and ASC-EV treatment protocol

All mouse experiments were carried out on C57BL/6J mice obtained from Charles River Laboratories, (Wilmington, MA, USA). All animals had the C57BL/6J genetic background (stock no. 000664). Chronic EAE was induced in female C57Bl/6J mice using an active immunization protocol. Briefly, animals were injected subcutaneously with 150 μg MOG35-55 peptide in 200 μL emulsion consisting of equal volumes of PBS and Complete Freund's Adjuvant (Becton Dickinson) supplemented with 1 mg *Mycobacterium tuberculosis* strain H37Ra (Becton Dickinson). Mice received 80 ng of pertussis toxin (Enzo Life Sciences, Farmingdale, NY, USA) intravenously at the time of immunization and 48 h later [36]. A previous titration to establish an optimal pertussis toxin dose for the induction of chronic EAE in C57BL/6J mice was performed [37]. All mice were weighed and examined daily for the neurological symptoms of EAE and scored according to the previously reported clinical scale [19]. The onset of the disease was considered when mice showed initial symptoms (limp tail) around 13 ± 3 days after immunization.

We decided to verify ASC-EV homing at disease onset because according to our previous data [19], ASC-EVs did not impact EAE development when injected after disease onset, but their preventive administration ameliorated the EAE course. ASC-EVs conjugated with USPIOs (40 μg of protein content corresponding to $6.07 \times 10^8 \pm 1.42$ particles) were injected intravenously at disease onset, and mice (n = 4) were killed after 48 h. EAE mice injected with USPIOs alone (n = 3) and healthy C57Bl/6J mice that did not receive subcutaneous immunization (n = 3) were considered controls.

Animals were housed in pathogen-free, climate-controlled facilities and provided with food and water *ad lib* according to current European Community laws. At the endpoints of all experiments, mice were deeply anesthetized and killed. All efforts were made to minimize suffering. All mouse experiments were carried out in accordance with experimental guidelines approved by the University of Verona committee on animal research (Centro Interdipartimentale di Servizio alla Ricerca Sperimentale) and the Italian Ministry of Health. All methods were completed and reported in accordance with the Animal Research: Reporting of *In Vivo* Experiments guidelines.

Magnetic resonance imaging

Magnetic resonance imaging (MRI) images were acquired using a tomograph (Bruker, Karlsruhe, Germany) equipped with a 4.7-T, 33-cm bore horizontal magnet (Oxford Ltd, Oxford, UK). Animals were anesthetized with 1% isoflurane inhalation in a mixture of oxygen and nitrogen and placed in prone position over a heated bed. Images were acquired with a cross-coil configuration. MRI acquisition was performed in EAE mice (n = 3) before intravenous administration of USPIO-EVs (pre-clinical stage around 12–13 days post-induction as previously reported by Farinazzo *et al.* [19]), the day of USPIO-EV injection (onset of disease) and 48 h post-USPIO-EV injection. EAE control mice (n = 3) received PBS. In order to detect USPIO-EVs, T2* map images were acquired using a multi-gradient echo sequence with repetition time of 2000 ms, echo time of 4.4 ms, field of view of 4.5×2 cm^2, matrix size of 288/128, slice thickness of 0.75 mm, n° of slice of 36, number of averages of 4 and total acquisition time of 12 min 48 s.

Histology

The presence of ASC-EVs labeled with USPIOs was verified by histological analysis of frozen sections of lymph nodes, lung, spleen and spinal cord of EAE-induced (n = 4 EAE mice injected with USPIO-EVs and n = 4 EAE mice injected with USPIOs alone) and healthy (n = 3) mice. To evaluate EV localization, Prussian Blue staining was performed. Sections were incubated with Prussian Blue solution (5% hydrochloric acid and 5% potassium ferrocyanide) for 40 min and counterstained with Nuclear Fast Red for 10 min. Sections were examined with an AxioPhot microscope equipped with an AxioCam HRc camera and AxioVision software (Zeiss, Oberkochen, Germany). Images were acquired from representative sections of 20 μm of lymph nodes per mouse collected every 100 μm for a total of 20–30 sections for each animal.

Electron microscopy

The morphology and size of USPIO-EVs and EVs were confirmed by the electron microscopy technique. For detection of the ultrastructural morphology of USPIO-EVs, EVs were embedded in agarose gel fixed in a solution of 2.5% glutaraldehyde plus 2% paraformaldehyde in 0.1 M phosphate buffer. All samples were post-fixed in 1% osmium tetroxide for 2 h. The sections were then dehydrated in graded concentrations of acetone and embedded in an Epon–Araldite mixture (Electron Microscopy Sciences, Hatfield, PA, USA). The ultrathin sections were cut with an Ultracut E microtome (Reichert, Vienna, Austria) at 70-nm thickness and placed on copper/rhodium grids. Transmission electron microscopy (TEM) images were acquired with a Morgagni transmission electron microscope (Philips, Amsterdam, the Netherlands) operating at 80 kV and equipped with a Megaview II camera (Philips) for digital image acquisition [33].

Vesicle samples (without USPIOs) were resuspended in 4% paraformaldehyde. A drop of solution was spotted onto a nickel mesh and air-dried. The grids were washed in PBS and fixed with 1% glutaraldehyde. Grids were then washed twice with PBS and stained with 1% uranyl acetate (Sigma-Aldrich, St Louis, MO, USA) for 10 min. Finally, the grids were air-dried and observed with a Zeiss EM 109 electron microscope; images were acquired via scanner (Perfection 4990 Photo; Epson, Suwa, Japan).

Lymph nodes and spinal cord from both EAE (n = 2) and healthy (n = 2) mice treated with USPIO-EVs and PBS, respectively, were dissected out and fixed with 2.5% glutaraldehyde in phosphate buffer for 1 h at 4°C and post-fixed in osmium tetroxide for 2 h at 4°C. The samples were subsequently dehydrated in acetone and embedded in Spurr resin. The ultrathin sections were cut at a thickness of 80 nm at three different levels of 100 μm and placed on copper/rhodium grids with an Ultracut E microtome (Reichert-Jung, Heidelberg, Germany). Samples were observed using an energy-filtered transmission electron microscope (Leo 912ab; Zeiss) operating at 80 kV, and digital images were acquired using an Esivision CCD-BM/1K system (Olympus, Germany).

Flow cytometry

Flow cytometry analysis was performed on the lymph nodes of both EAE and healthy mice treated with hEVs. Lymph nodes were mechanically dissected out and disrupted with a syringe and filtered through 80-μm nylon mesh. Cells were counted using a hemocytometer and assessed for viability using Trypan Blue. A total of 1×10^6 cells from lymph nodes of EAE and healthy mice were collected and resuspended in 1% bovine serum albumin in PBS. The cells were centrifuged at 300 × g for 5 min, the supernatant was removed and the pellet was resuspended in 100 μL of 1% bovine serum albumin in PBS. The following antibodies were added to the solution and incubated for 1 h in the dark at room temperature: CD16/CD32

unconjugated blocking agent, mouse anti-F480-FITC, CD45 APC-Cy7, B220 V450, CD8 V500, CD4 PerCP-Cy5.5 and CD11c-APC. All antibodies were purchased from Thermo Fisher Scientific and used at appropriate dilution. After centrifugation at 300 × g for 5 min, a FIX & PERM Cell Permeabilization Kit (Thermo Fisher Scientific) was used with or without (fluorescence minus one) anti-human HLA PE-Cy7 (clone w6/32; Thermo Fisher Scientific), which recognizes an antigenic determinant shared among products of the HLA-A, HLA-B and HLA-C loci. A flow cytometry gating strategy was used to define cell populations of interest as follows: (i) selection of viable cells was performed using light scatter properties to discard debris and doublets and (ii) selection of either CD45+ or CD45− cells to analyze different subsets of cells with markers of immunophenotype (lymphocyte B CD45+ and B220+, lymphocyte T D45+CD4 +/− CD8 −/+, macrophages F480+ B220−, dendritic cells CD11c+ CD45 subset +). A BD FACSCanto II (Becton Dickinson) was used at a low rate for the reading.

Statistical analysis

Statistical analysis was performed using a two-tailed Student's *t*-test. $P < 0.05$ was considered statistically significant.

Results

Characterization of EVs

In the present study, EVs were labeled with USPIOs (USPIO-EVs) starting from the loading of their parent cells. After EV extraction, the vesicles were able to retain small iron particles, as previously observed [33]. TEM images showed the presence of small iron particles inside EVs after their extraction from USPIO-loaded ASCs (Figure 1A). The presence of USPIOs in EVs did not impact on the typical characteristics of EVs in terms of morphology, as revealed by round vesicles with lipid bilayers with a diameter less than 130 nm (Figure 1B) [38,39] as well as protein content, size and concentration (Figure 1C–E). EVs and USPIO-EVs were analyzed and quantified by NTA (Table 1; also see supplementary Figure 1). Measurements were in line with the literature [38]. By western blot, we validated the presence of typical markers of EVs [40] identified on USPIO-EVs through CD9, TSG 101 and HSP-70 antibodies, which displayed specific signals at 25 kDa, 44 kDa and 70 kDa, respectively. GM130 was used to exclude the presence of components derived from Golgi apparatus (Figure 1F).

Homing and migration of USPIO-EVs in EAE mice

To verify the ability of USPIO-EVs to migrate to inflammatory sites following intravenous injection at EAE onset, a preliminary MRI analysis was performed at 48 h post-injection. EAE mice injected with USPIO-EVs showed lower T2* relaxation time values in lymph nodes compared with EAE mice injected with PBS (see supplementary Figure 2). These data are in line with a previous study in which USPIOs were used to detect EVs *in vivo* [33], confirming lymph nodes as the target site of ASC-EVs in EAE pathology [19]. To better characterize ASC-EVs with direct evidence, histological analysis of draining lymph nodes (both axillary and inguinal) was performed. Prussian Blue staining showed the presence of USPIO-EVs in the lymph nodes of EAE mice injected with USPIO-EVs (Figure 2A,B) but not in those of EAE mice injected with USPIOs alone (Figure 2C,D) or healthy animals injected with USPIO-EVs (Figure 2E,F). No signal was detected in the lung or spinal cord of EAE mice injected with USPIO-EVs (Figure 2G, H). No clear positivity was observed with Prussian Blue staining with regard to the spleen because of the presence of high endogenous iron deposits (data not shown) [41].

Formal and direct confirmation of the capacity of USPIO-labeled EVs to migrate to lymph nodes after systemic injection was obtained by TEM, which represents the gold standard for identifying small nanoparticles in tissues [42]. However, the technique is very time-consuming, so we focused our attention mainly on lymph nodes (our first and foremost identified target) and spinal cord (the major site involved in EAE pathology). The presence of iron particles was evidenced in the lymph nodes of EAE mice but not in the spinal cord (Figure 3F). Iron particles of round shape and expected size were observed in EAE mice injected with USPIO-EVs (Figure 3A–C) but not in those injected with USPIOs alone (Figure 3D,E).

Identification of cell targets of EVs in lymph nodes of EAE mice

The demonstration of the presence of ASC-EVs in the lymph nodes of EAE mice prompted us to investigate their cellular target. For this purpose, we injected hEVs (characterized by the expression of typical EV markers and HLA expression) (see supplementary Figure 3A,B) intravenously in EAE and healthy mice and analyzed by flow cytometry the cell populations present in the lymph nodes to verify which cell type contained hEVs. The presence of HLA signals in murine cells identified the incorporation of hEVs (Figure 4A–C).

As expected, given their phagocytic nature, F480+ macrophages and CD11c+ dendritic cells displayed the highest absolute HLA signal in the steady state as well as in the course of EAE induction compared with the other cells analyzed (Figure 4C). In particular, flow cytometry analysis showed a significant presence of HLA+ signal in F480+ macrophages, with a 1.45-fold increase in mean fluorescence intensity in EAE mice compared with healthy mice ($P = 0.0269$) (Figure 4D). Interestingly, albeit not statistically significant, probably due to the small number of animals processed, CD4+ T cells displayed a remarkably higher capacity to directly incorporate and accumulate hEVs in reactive lymph nodes (2.07-fold increase in mean fluorescence intensity in EAE mice compared with healthy mice), whereas no significant difference in HLA+ signal was observed in CD8+ T-cell and B lymphocyte populations of EAE lymph nodes compared with naive lymph nodes.

Discussion

In our current study, as in our previous studies [3,19], we exploited active immunization with MOG35-55 peptide as a myelin antigen using C57Bl/6J mice that develop a chronic model of EAE. Specifically, we evaluated (i) lymph nodes draining the immunization site, as a point of peripheral activation of myelin-specific T cells [43]; (ii) lungs, as sites where activated T cells become licensed to enter the CNS [44]; and (iii) spinal cord, as the main site of inflammation in this animal model of EAE [43]. The labeling strategy of EVs with USPIOs not only represents a feasible approach for *in vivo* spatiotemporal tracking but could also be used to investigate EV biology and composition, facilitating and promoting the identification of new pro-inflammatory targets.

First, to address the tissue accumulation of ASC-EVs, we evaluated their distribution, comparing healthy and EAE-induced mice 48 h after intravenous injection of USPIO-labeled vesicles. For this purpose, the presence of USPIO-EVs was investigated by Prussian Blue histochemical staining and the obtained data were confirmed by TEM. Retention of iron deposits was found in the lymph nodes of EAE mice but not in the lungs. Moreover, although EVs have a lipidic nature and can potentially cross the blood–brain barrier, no evidence of iron retention was detected in the spinal cord. These results highlight the EV accumulation in secondary lymphoid organs and could suggest a disease-associated phenomenon aimed at modulating peripheral T lymphocyte activation, a process characterizing the establishment of T-cell-based CNS inflammation [45]. This evidence is in line with our previous study, in which ASC-EVs preferentially exerted an anti-inflammatory effect in lymphoid organs rather than within the CNS [19]. Surprisingly, we did not detect EVs in the

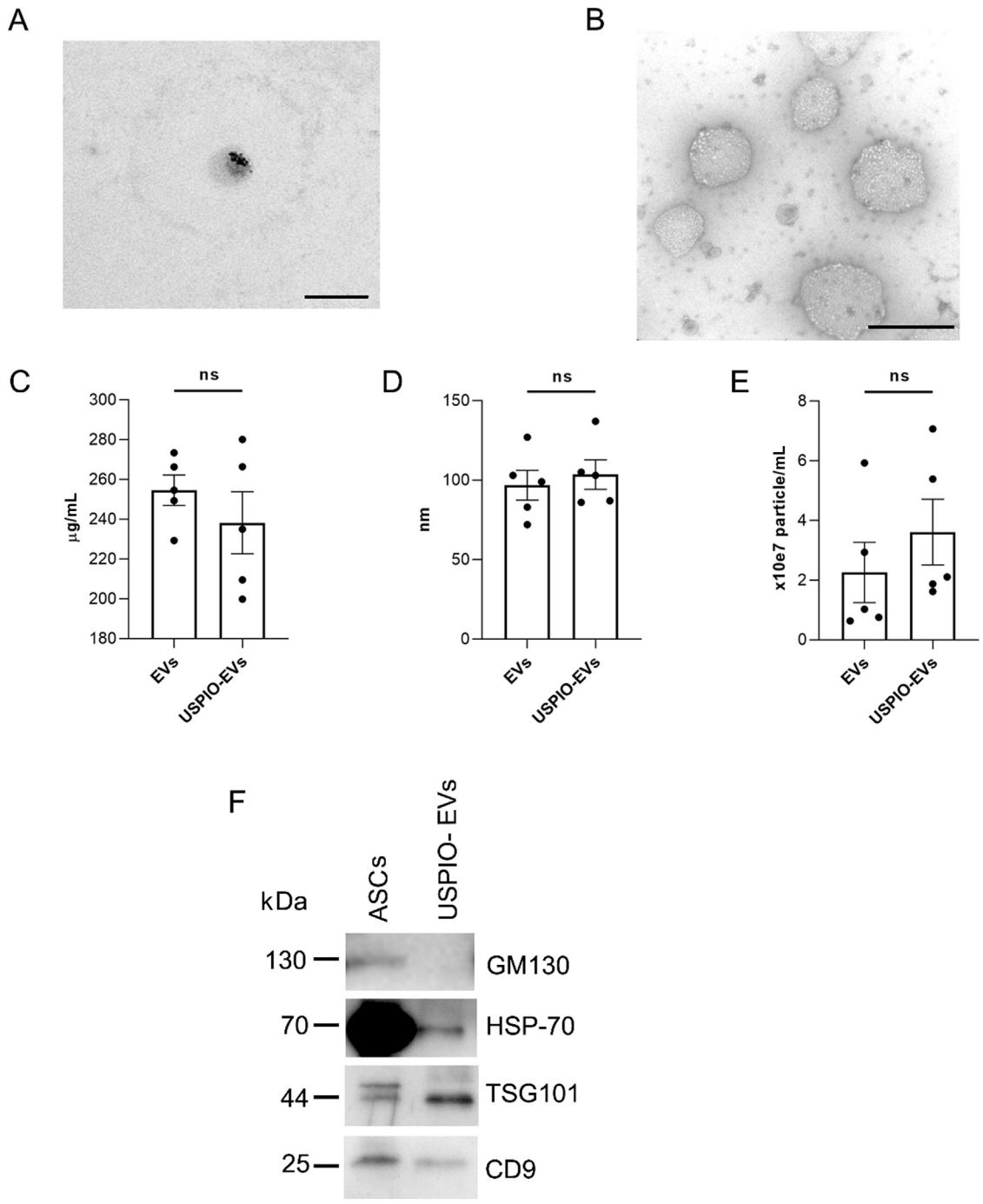

Figure 1. Characterization of murine EVs. (A) High TEM magnification of USPIO-EVs in phantom gel showed the labeling of a single vesicle loaded with iron particles after extraction from ASCs (scale bar = 100 nm). (B) Representative TEM images of EVs showed particles with characteristic morphology and size (scale bar = 100 nm). (C) Protein concentration of EVs and USPIO-EVs was detected by BCA protein assay (n = 5). Analysis was performed using Student's *t*-test, and data are shown as mean ± SEM. (D) Mode particle diameter of EVs and USPIO-EVs measured and analyzed by NTA (n = 5). Analysis was performed using Student's *t*-test, and data are shown as mode ± SEM. (E) Concentration of EVs and USPIO-EVs was measured and analyzed by NTA (n = 5). (F) Western blot analysis of specific EV protein markers. In USPIO-EV fraction, bands were present at 25 kDa, 44 kDa and 70 kDa after incubation with CD9, TSG101 and HSP70 antibodies, respectively. GM130 was used to exclude the presence of components derived from Golgi apparatus. ASC lysates were used as a positive control. BCA, bicinchoninic acid; ns, not significant; $P>0.05$; SEM, standard error of the mean. All reported "n" represent biological replicates.

Table 1
Summary data of NTA.

Sample	Mean diameter, nm	Mode diameter, nm	d90/d10	Raw concentration, particles/mL	Particle count	Particle rate, particles/min
EVs (n = 5)	132.8 ± 5.35	92.1 ± 5.4	4.15 ± 1.11	$2.25 \times 10^7 \pm 1.009$	4.04 ± 1.84	1580.0 ± 816.73
USPIO-EVs (n = 5)	123.6 ± 7.2	109.4 ± 8.7	3.02 ± 0.62	$3.6 \times 10^7 \pm 1.103$	6.7 ± 2.1	2083.2 ± 759.44

Data represent the analysis of USPIO-EVs and EVs alone after extraction from murine ASCs. Data are reported as mean ± standard error of the mean (n = 5). There are no statistically significant differences for reported parameters. For diameter of particles, both average and mode are reported. All reported "n" represent 5 different batches of ASC-EVs.

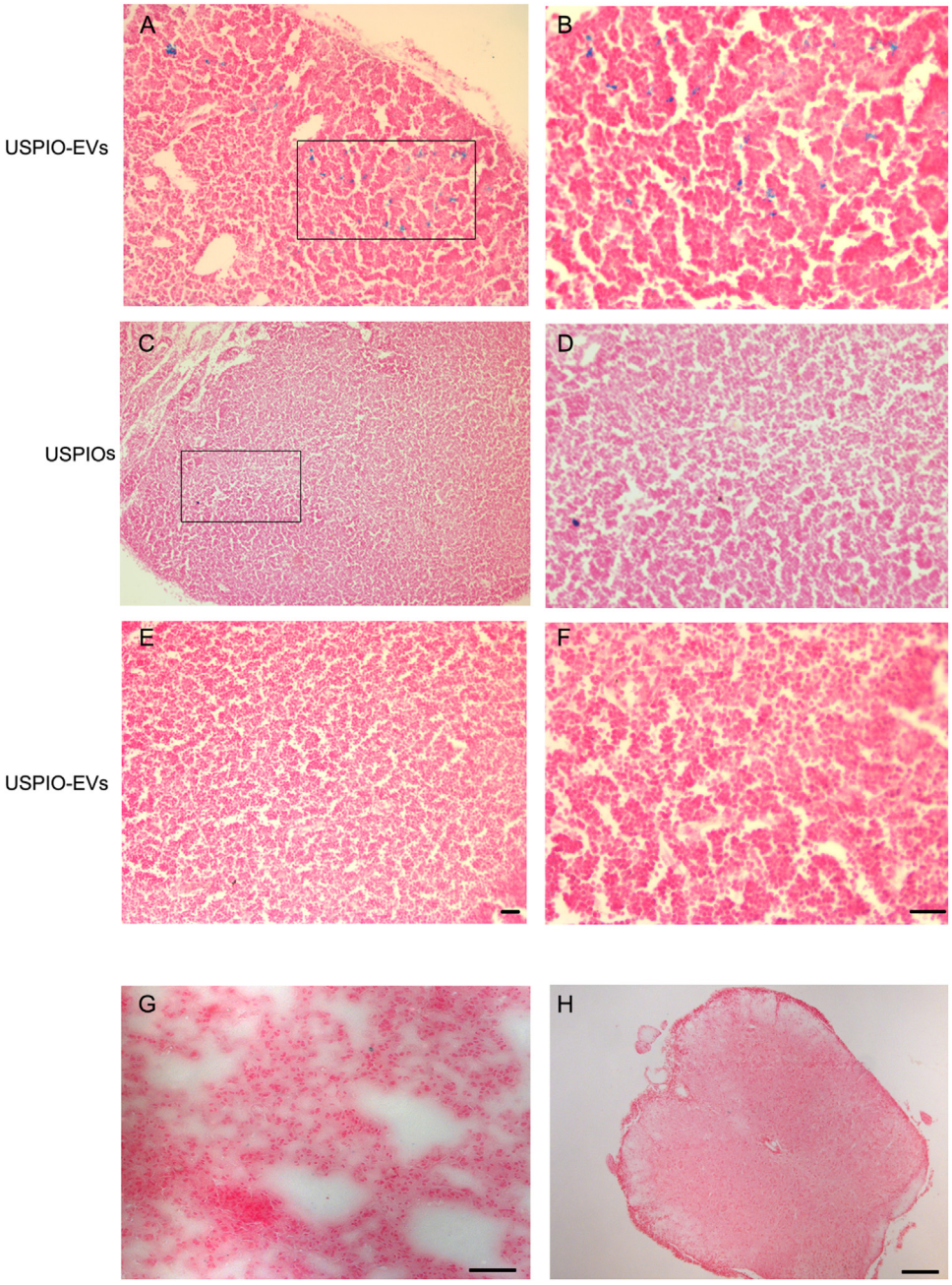

Figure 2. Identification of USPIO-EV homing in EAE. Histological analysis of axillary lymph nodes of EAE mice. (A) Prussian Blue staining revealed the presence of signal in the lymph nodes of EAE mice injected with USPIO-EVs (magnification 20X; scale bar = 50 μm). (B) Higher magnification 40X(scale bar = 50 μm). (C) No positivity was observed in EAE mice injected with USPIOs alone (magnification 20X; scale bar = 50 μm). (D) Higher magnification 40X(scale bar = 50 μm). (E) No signals were observed in healthy mice injected with USPIO-EVs (magnification 20X; scale bar = 50 μm). (F) Higher magnification 40X(scale bar = 50 μm). (G) No particles were observed in the lungs of EAE mice injected with USPIO-EVs (scale bar = 100 μm). (H) No particles were observed in the spinal cord of EAE mice injected with USPIO-EVs (scale bar = 200 μm).

lymph nodes of healthy mice 48 h after intravenous injection. With respect to this, using human ovarian cancer-derived vesicles, it was clearly demonstrated how these EVs could be actively transported by lymphatic endothelial cells from the interstitial flow into the lymphatic vessel [46]. We can therefore suppose that systemic and local inflammatory conditions that arise in the early phases of EAE could accelerate the widespread dissemination of EVs from vascular-activated endothelium and, at the same time, facilitate their lymphatic drainage, uptake and retention in inflamed lymph nodes in the full course of T-cell priming. This is the first direct evidence of the preferential uptake and retention of EVs in draining lymph nodes during EAE.

We then moved our efforts to assessing the potential cellular target of ASC-EVs in this experimental paradigm. To this end, we treated mice with hEVs, using HLA [47] as a marker to discriminate human-derived vesicles within mouse tissues. In particular, we compared the draining lymph nodes of EAE mice with those obtained from healthy mice, here used to quantify basal HLA signal. First, we analyzed T and B lymphocytes, which are the most prominent cell types in lymph nodes during EAE [43]. B lymphocytes were found to be those that incorporated the least amount of EVs compared with the other cell populations analyzed. However, a recent study highlighted how the modulatory effect of MSCs on B cells is independent of EV secretion [48].

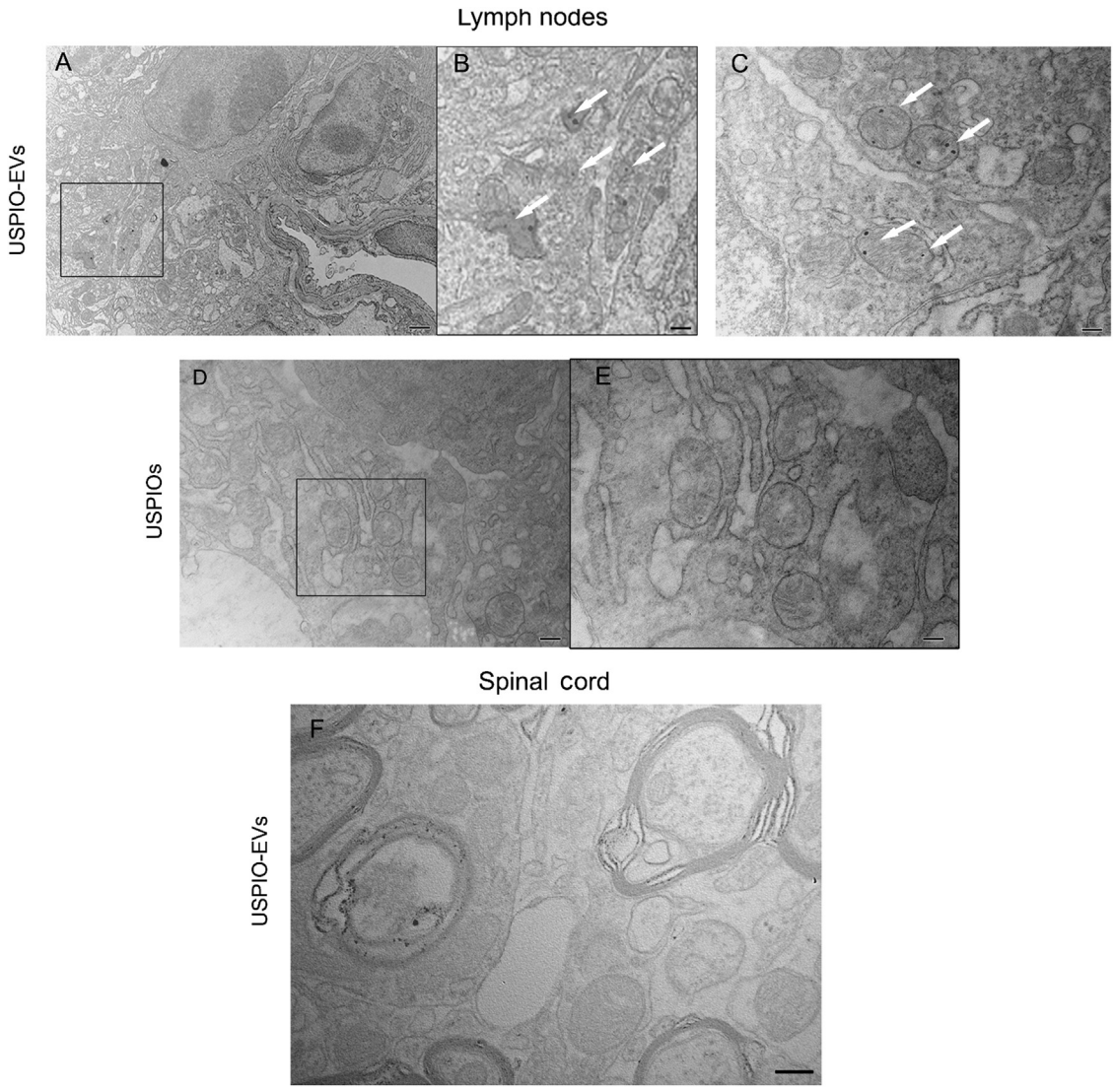

Figure 3. Ultrastructural study of USPIO-EVs in EAE mice. (A,C) TEM analysis of lymph nodes of EAE mice injected with USPIO-EVs revealed the presence of nanoparticles of the expected size (scale bar = 1 μm). (B) Higher magnification (scale bar= 1μm). (D) No signal was observed in lymph nodes of EAE mice when USPIOs alone were injected. (E) Higher magnification (scale bar = 200 nm). (F) No signal was observed in spinal cord of EAE mice injected with USPIO-EVs.

In contrast to B cells, CD4+ T lymphocytes showed a higher ability to internalize EVs in lymph nodes during EAE induction compared with a steady state. These data are in line with our previous study, demonstrating how direct *in vitro* treatment with ASC-EVs was sufficient to modulate MOG35-55-activated T cells, suppressing their adhesion to CNS pial vessels by inhibiting integrin-dependent chemokine signaling [19].

Interestingly, we observed a significant load of EVs in F480+ macrophages combined with moderate accumulation in CD11c+ dendritic cells. Notably, recent experimental evidence indicates that lymphoid tissue-resident macrophages are pivotal contributors to the creation of the inflammatory response in the context of autoimmune diseases [49]. In particular, these macrophages are the main cell type able to capture antigens—and even EVs—from lymph and blood. This process prevents further antigen dissemination and, upon antigen transfer to dendritic cells, enables the local shaping of an adaptive immune response [50]. The ability of macrophages to internalize ASC-derived small vesicles was recently demonstrated both *in vitro* and *in vivo* in different pathological conditions [51,52]. In these cells, EVs promote anti-inflammatory M2 polarization, enhancing homeostasis restoration and functional outcomes [51,53]. Dendritic cell cross-talk with T cells within antigen-draining lymph nodes represents the initiating step for generating a productive adaptive immune response [54]. Shahir *et al.* [55] have recently demonstrated how murine ASC-EVs can suppress the maturation of *in vitro* differentiated dendritic cells and stimulate the release of anti-inflammatory cytokines, thus promoting an immunological tolerance status. An *in vitro* modulatory effect on dendritic cells was also observed using human bone marrow-derived MSC-EVs [56]. These data, together with the presence of EVs we found internalized by dendritic cells in the lymph nodes of EAE-induced mice, are perfectly in accordance with our previous study [19]. We have indeed reported a partial but significant reduction in T-cell proliferation and cytokine release in the lymph nodes of EAE mice that received a preventive ASC-EV treatment. These data suggest a potential translational application of intravenous administration of ASC-EVs to human therapy in order to prevent or attenuate MS relapses by their immunomodulatory effect, as clinically applied for several oral and infusible disease-modifying therapies [57,58]. Moreover, the systemic immunosuppressive properties of MSCs were demonstrated using different animal models of autoimmune disorders, such as autoimmune type 1 diabetes [59], lupus [60], graft-versus-host disease [61] and rheumatoid arthritis [62–64], suggesting a potential translational therapeutic application of ASC-EVs in managing autoimmunity.

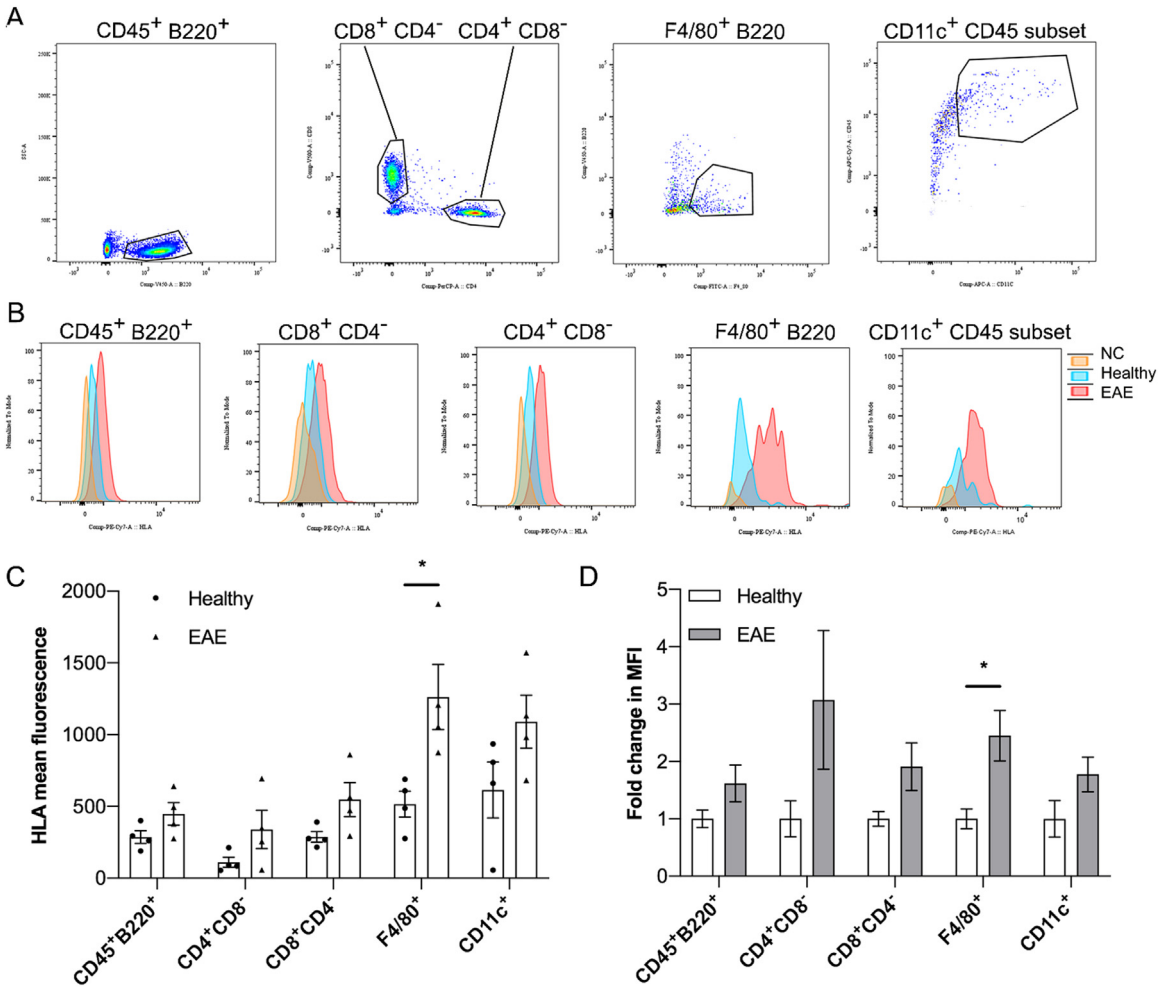

Figure 4. Cellular target of ASC-EVs in EAE mice. Flow cytometry analysis of lymph nodes for the identification of cellular target of hEVs in EAE and healthy mice. (A) Representative dot plots showing the gating strategy to identify different cellular populations. (B) Histograms of the intensity of HLA signal relative to hEVs in different subpopulations of lymph nodes. (C) MFI of HLA+ cells in different subpopulations of lymph nodes. (D) MFI fold change in macrophages and dendritic cells in EAE mice compared with healthy mice. Analysis was performed using Student's *t*-test, and data are shown as mean ± SEM (n = 4). $^*P < 0.05$. MFI, mean fluorescence intensity; NC, negative control; SEM, standard error of the mean.

One of the limitations of this study is the low number of animals enrolled; however, the purpose was to verify the distribution of ASC-EVs from blood to peripheral tissues during the acute phase of EAE. The data that have been obtained will allow to better focalize succeeding studies on the molecular mechanisms exerted by ASC-EVs on peripheral immunity during the early onset of inflammatory autoimmune disorders of the CNS. Moreover, future experiments will be needed to clarify whether interfering with ASC-EV uptake by the immune cells within inflamed lymph nodes could affect the clinical manifestation of EAE. Several studies have demonstrated the role of ASC-EVs in nerve regeneration, neuronal protection, synaptic plasticity and remyelination, indicating a possible therapeutic potential of these vesicles in the treatment of chronic neurodegenerative diseases [15,59]. In this regard, because of the undetectable number of vesicles spread from the circulation to the CNS, intravenous administration of ASC-EVs represents another limitation. This restriction could partially explain the lack of benefit in terms of clinical symptoms we observed in the therapeutic administration protocol [19] and hence the need to develop different therapeutic treatments with more effective administration protocols with regard to directing EVs into the CNS. In this respect, it has been demonstrated that nanovesicles, including ASC-EVs, can cross the blood–brain barrier if administered intranasally [14,65,66] and that intranasal delivery of different stem cells is effective in animal models of subarachnoid hemorrhage [67], stroke [68], spinal cord injury [66] and MS [65,69], suggesting that this route of administration is an efficient delivery system for treating CNS disorders, including MS.

Conclusions

Taken together, our results indicate that ASC-EVs injected intravenously specifically reach draining lymph nodes in EAE mice at early stages of the disease—remarkably, when the immune response is mounting. In this context, ASC-EVs are mainly incorporated by macrophages and dendritic cells. The identification of draining lymph nodes could represent a possible target of ASC-EVs to be taken into consideration for the development of future ASC-EV therapeutic strategies. Further studies are necessary to address the possibility that ASC-EVs reach the CNS at different time points or through different delivery routes. These results represent a corollary to our previous, more clinical and mechanistic study [19] and provide new insights into the migratory capacity of ASC-EVs in EAE, which could be exploited for the future therapeutic use of ASC-EVs.

Funding

This research was supported in part by a grant from Fondazione Italiana Sclerosi Multipla (BB; grant no. 2016/R/1).

Declaration of Competing Interest

The authors have no commercial, proprietary or financial interest in the products or companies described in this article.

Author Contributions

Conception and design of the study: GC, RM and BB. Acquisition of data: ET, IS, RB, SD, GA, NL and GM. Analysis and interpretation of data: ET, IS, RB, SD, GA, NL and GM. Drafting or revising the manuscript: ET, BR, RF and BB. All authors have approved the final article.

Acknowledgments

The authors thank Unitech Nolimits of Università degli studi di Milano and Manuela Malatesta of Università degli studi di Verona for their assistance with the TEM images. The authors are grateful to Alessandro Mattè for his help with flow cytometry assay and to Centro Piattaforme Tecnologiche of Università degli studi di Verona for technical assistance. The authors also thank Federica Virla and Ugo Postiglione for editing support.

Ethics Statement

The study was conducted according to the guidelines of the Declaration of Helsinki and approved by the ethics committee of the University of Verona (protocol no. 12269, authorization no. 107/2014-PR, approval date December 19, 2014).

Supplementary materials

Supplementary material associated with this article can be found in the online version at doi:10.1016/j.jcyt.2023.12.007.

References

[1] Thompson AJ, et al. Multiple sclerosis. Lancet 2018;391(10130):1622–36.
[2] Correale J, Marrodan M, Ysrraelit MC. Mechanisms of Neurodegeneration and Axonal Dysfunction in Progressive Multiple Sclerosis. Biomedicines 2019;7(1):14.
[3] Constantin G, et al. Adipose-derived mesenchymal stem cells ameliorate chronic experimental autoimmune encephalomyelitis. Stem Cells 2009;27(10):2624–35.
[4] Gerdoni E, et al. Mesenchymal stem cells effectively modulate pathogenic immune response in experimental autoimmune encephalomyelitis. Ann Neurol 2007;61(3):219–27.
[5] Kassis I, et al. Neuroprotection and immunomodulation with mesenchymal stem cells in chronic experimental autoimmune encephalomyelitis. Arch Neurol 2008;65(6):753–61.
[6] Morando S, et al. The therapeutic effect of mesenchymal stem cell transplantation in experimental autoimmune encephalomyelitis is mediated by peripheral and central mechanisms. Stem Cell Res Ther 2012;3(1):3.
[7] Zappia E, et al. Mesenchymal stem cells ameliorate experimental autoimmune encephalomyelitis inducing T-cell anergy. Blood 2005;106(5):1755–61.
[8] Jiang H, et al. Amelioration of experimental autoimmune encephalomyelitis through transplantation of placental derived mesenchymal stem cells. Sci Rep 2017;7:41837.
[9] Lavoie JR, Rosu-Myles M. Uncovering the secretes of mesenchymal stem cells. Biochimie 2013;95(12):2212–21.
[10] Marconi S, et al. Systemic treatment with adipose-derived mesenchymal stem cells ameliorates clinical and pathological features in the amyotrophic lateral sclerosis murine model. Neuroscience 2013;248:333–43.
[11] Wei X, et al. Adipose stromal cells-secreted neuroprotective media against neuronal apoptosis. Neurosci Lett 2009;462(1):76–9.
[12] Baglio SR, et al. Human bone marrow- and adipose-mesenchymal stem cells secrete exosomes enriched in distinctive miRNA and tRNA species. Stem Cell Res Ther 2015;6:127.
[13] Bonafede R, et al. Exosome derived from murine adipose-derived stromal cells: Neuroprotective effect on *in vitro* model of amyotrophic lateral sclerosis. Exp Cell Res 2016;340(1):150–8.
[14] Bonafede R, et al. ASC-Exosomes Ameliorate the Disease Progression in SOD1 (G93A) Murine Model Underlining Their Potential Therapeutic Use in Human ALS. Int J Mol Sci 2020;21(10):3651.
[15] Farinazzo A, et al. Murine adipose-derived mesenchymal stromal cell vesicles: *in vitro* clues for neuroprotective and neuroregenerative approaches. Cytotherapy 2015;17(5):571–8.
[16] Liu W, et al. Exosomes Derived from Bone Mesenchymal Stem Cells Repair Traumatic Spinal Cord Injury by Suppressing the Activation of A1 Neurotoxic Reactive Astrocytes. J Neurotrauma 2019;36(3):469–84.
[17] Long Q, et al. Intranasal MSC-derived A1-exosomes ease inflammation, and prevent abnormal neurogenesis and memory dysfunction after status epilepticus. Proc Natl Acad Sci U S A, 2017;114(17):E3536–45.
[18] Fayazi N, et al. Stem Cell-Derived Exosomes: a New Strategy of Neurodegenerative Disease Treatment. Mol Neurobiol 2021;58(7):3494–514.
[19] Farinazzo A, et al. Nanovesicles from adipose-derived mesenchymal stem cells inhibit T lymphocyte trafficking and ameliorate chronic experimental autoimmune encephalomyelitis. Sci Rep 2018;8(1):7473.
[20] Nasri F, et al. Therapeutic Efficacy of Mesenchymal Stem Cells and Mesenchymal Stem Cells-derived Neural Progenitors in Experimental Autoimmune Encephalomyelitis. Int J Stem Cells 2018;11(1):68–77.
[21] Busato A, et al. Labeling and Magnetic Resonance Imaging of Exosomes Isolated from Adipose Stem Cells. Curr Protoc Cell Biol 2017;75:3.44.1–3.44.15.
[22] Perets N, et al. Golden Exosomes Selectively Target Brain Pathologies in Neurodegenerative and Neurodevelopmental Disorders. Nano Lett 2019;19(6):3422–31.
[23] Cao H, et al. *In Vivo* Tracking of Mesenchymal Stem Cell-Derived Extracellular Vesicles Improving Mitochondrial Function in Renal Ischemia-Reperfusion Injury. ACS Nano 2020;14(4):4014–26.
[24] Betzer O, et al. *In Vivo* Neuroimaging of Exosomes Using Gold Nanoparticles. ACS Nano 2017;11(11):10883–93.
[25] Uccelli A, et al. Safety, tolerability, and activity of mesenchymal stem cells versus placebo in multiple sclerosis (MESEMS): a phase 2, randomised, double-blind crossover trial. Lancet Neurol 2021;20(11):917–29.
[26] Direkze NC, et al. Bone marrow contribution to tumor-associated myofibroblasts and fibroblasts. Cancer Res 2004;64(23):8492–5.
[27] Roorda BD, et al. Mesenchymal stem cells contribute to tumor cell proliferation by direct cell-cell contact interactions. Cancer Invest 2010;28(5):526–34.
[28] Peroni D, et al. Stem molecular signature of adipose-derived stromal cells. Exp Cell Res 2008;314(3):603–15.
[29] Dominici M, et al. Minimal criteria for defining multipotent mesenchymal stromal cells. The International Society for Cellular Therapy position statement. Cytotherapy 2006;8(4):315–7.
[30] Krampera M, et al. Induction of neural-like differentiation in human mesenchymal stem cells derived from bone marrow, fat, spleen and thymus. Bone 2007;40(2):382–90.
[31] Krampera M, et al. HB-EGF/HER-1 signaling in bone marrow mesenchymal stem cells: inducing cell expansion and reversibly preventing multilineage differentiation. Blood 2005;106(1):59–66.
[32] Marconi S, et al. Human adipose-derived mesenchymal stem cells systemically injected promote peripheral nerve regeneration in the mouse model of sciatic crush. Tissue Eng Part A 2012;18(11-12):1264–72.
[33] Busato A, et al. Magnetic resonance imaging of ultrasmall superparamagnetic iron oxide-labeled exosomes from stem cells: a new method to obtain labeled exosomes. Int J Nanomedicine 2016;11:2481–90.
[34] Shelke GV, et al. Importance of exosome depletion protocols to eliminate functional and RNA-containing extracellular vesicles from fetal bovine serum. J Extracell Vesicles 2014;3(1):24783.
[35] Davies R, et al. Extracellular Vesicle Depletion Protocols of Foetal Bovine Serum Influence Umbilical Cord Mesenchymal Stromal Cell Phenotype, Immunomodulation, and Particle Release. Int J Mol Sci 2023;24(11):9242.
[36] Dusi S, et al. LFA-1 Controls Th1 and Th17 Motility Behavior in the Inflamed Central Nervous System. Front Immunol 2019;10:2436.
[37] Huntemann N, et al. An optimized and validated protocol for inducing chronic experimental autoimmune encephalomyelitis in C57BL/6J mice. J Neurosci Methods 2022;367:109443.
[38] Doyle LM, Wang MZ. Overview of Extracellular Vesicles, Their Origin, Composition, Purpose, and Methods for Exosome Isolation and Analysis. Cells 2019;8(7):727.
[39] Raposo G, Stoorvogel W. Extracellular vesicles: exosomes, microvesicles, and friends. J Cell Biol 2013;200(4):373–83.
[40] Kowal J, et al. Proteomic comparison defines novel markers to characterize heterogeneous populations of extracellular vesicle subtypes. Proc Natl Acad Sci U S A, 2016;113(8):E968–77.
[41] Miller MA, Zachary JF. Mechanisms and Morphology of Cellular Injury, Adaptation, and Death. Pathologic Basis of Veterinary Disease 2017: 2–43.e19.
[42] Malatesta M. Transmission Electron Microscopy as a Powerful Tool to Investigate the Interaction of Nanoparticles with Subcellular Structures. Int J Mol Sci 2021;22(23):12789.
[43] Barthelmes J, et al. Induction of Experimental Autoimmune Encephalomyelitis in Mice and Evaluation of the Disease-dependent Distribution of Immune Cells in Various Tissues. J Vis Exp 2016;8(111):53933.
[44] Odoardi F, et al. T cells become licensed in the lung to enter the central nervous system. Nature 2012;488(7413):675–9.
[45] Sonar SA, Lal G. Differentiation and Transmigration of CD4 T Cells in Neuroinflammation and Autoimmunity. Front Immunol 2017;8:1695.
[46] Srinivasan S, Vannberg FO, Dixon JB. Lymphatic transport of exosomes as a rapid route of information dissemination to the lymph node. Sci Rep 2016;6:24436.
[47] Blazquez R, et al. Immunomodulatory Potential of Human Adipose Mesenchymal Stem Cells Derived Exosomes on *in vitro* Stimulated T Cells. Front Immunol 2014;5:556.
[48] Carreras-Planella L, et al. Immunomodulatory Effect of MSC on B Cells Is Independent of Secreted Extracellular Vesicles. Front Immunol 2019;10:1288.
[49] Li Q, et al. CD169 Expressing Macrophage, a Key Subset in Mesenteric Lymph Nodes Promotes Mucosal Inflammation in Dextran Sulfate Sodium-Induced Colitis. Front Immunol 2017;8:669.

[50] Grabowska J, et al. CD169(+) Macrophages Capture and Dendritic Cells Instruct: The Interplay of the Gatekeeper and the General of the Immune System. Front Immunol 2018;9:2472.
[51] Liu Y, et al. AMSC-derived exosomes alleviate lipopolysaccharide/d-galactosamine-induced acute liver failure by miR-17-mediated reduction of TXNIP/NLRP3 inflammasome activation in macrophages. EBioMedicine 2018;36:140–50.
[52] Zhao H, et al. Exosomes From Adipose-Derived Stem Cells Attenuate Adipose Inflammation and Obesity Through Polarizing M2 Macrophages and Beiging in White Adipose Tissue. Diabetes 2018;67(2):235–47.
[53] Cho KS, et al. Dendritic cells and M2 macrophage play an important role in suppression of Th2-mediated inflammation by adipose stem cells-derived extracellular vesicles. Stem Cell Res 2019;39:101500.
[54] Eisenbarth SC. Dendritic cell subsets in T cell programming: location dictates function. Nat Rev Immunol 2019;19(2):89–103.
[55] Shahir M, et al. Effect of mesenchymal stem cell-derived exosomes on the induction of mouse tolerogenic dendritic cells. J Cell Physiol 2020;235(10):7043–55.
[56] Reis M, et al. Mesenchymal Stromal Cell-Derived Extracellular Vesicles Attenuate Dendritic Cell Maturation and Function. Front Immunol 2018;9:2538.
[57] Garg N, Smith TW. An update on immunopathogenesis, diagnosis, and treatment of multiple sclerosis. Brain Behav 2015;5(9):e00362.
[58] Farjam M, et al. Emerging immunopharmacological targets in multiple sclerosis. J Neurol Sci 2015;358(1-2):22–30.
[59] Lee RH, et al. Multipotent stromal cells from human marrow home to and promote repair of pancreatic islets and renal glomeruli in diabetic NOD/scid mice. Proc Natl Acad Sci U S A, 2006;103(46):17438–43.
[60] Zhou K, et al. Transplantation of human bone marrow mesenchymal stem cell ameliorates the autoimmune pathogenesis in MRL/lpr mice. Cell Mol Immunol 2008;5(6):417–24.
[61] Ringden O, et al. Mesenchymal stem cells for treatment of therapy-resistant graft-versus-host disease. Transplantation 2006;81(10):1390–7.
[62] Gonzalez MA, et al. Treatment of experimental arthritis by inducing immune tolerance with human adipose-derived mesenchymal stem cells. Arthritis Rheum 2009;60(4):1006–19.
[63] Bouffi C, et al. Skin fibroblasts are potent suppressors of inflammation in experimental arthritis. Ann Rheum Dis 2011;70(9):1671–6.
[64] Augello A, et al. Cell therapy using allogeneic bone marrow mesenchymal stem cells prevents tissue damage in collagen-induced arthritis. Arthritis Rheum 2007;56(4):1175–86.
[65] Wu S, et al. Intranasal Delivery of Neural Stem Cells: A CNS-specific, Non-invasive Cell-based Therapy for Experimental Autoimmune Encephalomyelitis. J Clin Cell Immunol 2013;4(3):142.
[66] Guo S, et al. Intranasal Delivery of Mesenchymal Stem Cell Derived Exosomes Loaded with Phosphatase and Tensin Homolog siRNA Repairs Complete Spinal Cord Injury. ACS Nano 2019;13(9):10015–28.
[67] Nijboer CH, et al. Intranasal Stem Cell Treatment as a Novel Therapy for Subarachnoid Hemorrhage. Stem Cells Dev 2018;27(5):313–25.
[68] Wei N, et al. Delayed intranasal delivery of hypoxic-preconditioned bone marrow mesenchymal stem cells enhanced cell homing and therapeutic benefits after ischemic stroke in mice. Cell Transplant 2013;22(6):977–91.
[69] Fransson M, et al. Intranasal delivery of central nervous system-retargeted human mesenchymal stromal cells prolongs treatment efficacy of experimental autoimmune encephalomyelitis. Immunology 2014;142(3):431–41.